

# Stacked Self-Assembled Cubic GaN Quantum Dots Grown by Molecular Beam Epitaxy

Sarah Blumenthal,\* Torsten Rieger, Doris Meertens, Alexander Pawlis, Dirk Reuter, and Donat J. As

We have investigated the stacking of self-assembled cubic GaN quantum dots (QDs) grown in Stranski–Krastanov (SK) growth mode. The number of stacked layers is varied to compare their optical properties. The growth is in situ controlled by reflection high energy electron diffraction to prove the SK QD growth. Atomic force and transmission electron microscopy show the existence of wetting layer and QDs with a diameter of about 10 nm and a height of about 2 nm. The QDs have a truncated pyramidal form and are vertically aligned in growth direction. Photoluminescence measurements show an increase of the intensity with increasing number of stacked QD layers. Furthermore, a systematic blue-shift of 120 meV is observed with increasing number of stacked QD layers. This blueshift derives from a decrease in the QD height, because the QD height has also been the main confining dimension in our QDs.

## 1. Introduction

Group III-nitrides attracted much attention in the development of optical and quantum optical devices, operating in the UV spectral range. Especially, quantum dots (QDs) are used for many applications like QD-lasers, single photon emitters, and QD-detectors. Stacking of the QDs is an appropriate way to increase the number of QDs in the active region. Due to the stacked QDs in three dimensions, quantum dot lasers are a promising candidate for optoelectronic devices.<sup>[1,2]</sup> In the last years, stacked hexagonal GaN (h-GaN) QDs have already been realized indicating an increase in room temperature photoluminescence intensity with increasing number of stacked QD layers.<sup>[3]</sup> However, the hexagonal phase

S. Blumenthal, Dr. D. Reuter, Dr. D. J. As  
Department of Physics  
University of Paderborn  
Warburger Str. 100, 33098 Paderborn, Germany  
E-mail: sarah.blumenthal@upb.de

Dr. T. Rieger, Dr. A. Pawlis  
Peter Grünberg Institut  
Forschungszentrum Jülich  
52428 Jülich, Germany

D. Meertens  
Ernst Ruska Centre for Microscopy and Spectroscopy with Electrons  
Forschungszentrum Jülich  
52428 Jülich, Germany

 The ORCID identification number(s) for the author(s) of this article can be found under <https://doi.org/10.1002/pssb.201600729>.

DOI: 10.1002/pssb.201600729

exhibits an internal field causing a reduced recombination probability.<sup>[4]</sup> This may be overcome by using zincblende cubic GaN (c-GaN), where no polarization fields in (001) growth direction exist.<sup>[5]</sup> Only few groups are working with this metastable phase. First results for QD stacking of c-GaN QDs is shown by Martinez-Guerrero et al.<sup>[6]</sup> Bürger et al.<sup>[7]</sup> already published the growth of a single layer of c-GaN QDs in SK growth mode. Single-photon emission from these QDs is also demonstrated.<sup>[8]</sup> The QDs show radiative lifetimes about one order of magnitude shorter compared to hexagonal, polar GaN QDs, which are emitting at the same energy.<sup>[9]</sup> The incorporation of these QDs into photonic structures, like microdisks and two-dimensional photonic crystal membranes with high quality factors is already realized.<sup>[10–12]</sup>

In the InAs/GaAs and InGaAs/GaAs system, the realization of stacked QDs embedding in microcavities led to an increase of the optical gain and resulted in lasing at a considerable lower subband at room temperature.<sup>[13]</sup> Vertical stacking of QDs with a thin spacer layer led to a coupling of the QD layers. This coupling induced vertical alignment of the dots,<sup>[14,15]</sup> due to local strain fields originated by the subjacent QD layer and prompted preferential nucleation sites vertically aligned in the subsequent layer. In addition to the influence on the structural properties, electronic properties may change due to the stacking of quantum dots. The reasons include a change of the strain<sup>[16]</sup> and electronic coupling between the quantum dot layers.<sup>[14,17]</sup> In the InAs system these effects resulted in a redshift in PL emission energy in most stacking experiments.<sup>[14,17]</sup> An exception is described by Heidemeyer et al.<sup>[16]</sup> They observed a blueshift in PL emission energy of a twofold stacked QD sample compared to the single layer and trace it back to a growth-related phenomenon as strain induced intermixing or indium loss and in addition to complex strain fields that exist in the closely stacked QDs.

In contrast to InAs/GaAs QDs, we observed a blueshift of the QD emission with increasing layers of stacks in our cubic GaN/AlN QD structures.

## 2. Experimental Section

Our samples are grown by molecular beam epitaxy (MBE). For gallium and aluminum evaporation, standard effusion cells are used. The nitrogen is derived from dissociation of N<sub>2</sub> using a

plasma cell. The substrate is a 10  $\mu\text{m}$  thick 3C-SiC layer on top of a 500  $\mu\text{m}$  Si (001) substrate (see **Figure 1**). The samples consist of a 14 nm thick c-AlN buffer layer. After growth of the c-AlN buffer layer, Ga and N shutter are opened simultaneously for 25 s (6 MLs). Subsequently, both Ga and N-shutters are closed. During this deposition the c-GaN QDs are grown employing the self-assembled Stranski–Krastanov (SK) growth. This growth mechanism is due to a lattice mismatch of 3.2% between c-AlN and c-GaN. After transformation, cubic GaN QDs on top of an about 2 ML thick wetting layer are formed. After the deposition of GaN a break of about 15 s is introduced and then the growth of the c-AlN spacer layer started. For this layer Al and N shutter are opened simultaneously. It is not clear yet, if there is any difference of growing on top of the substrate or on top of the c-GaN QD layer. The growth rate during the growth of the first few MLs might be different for the different sub materials (3C-SiC for the first layer and c-GaN for the upper layers).

The growth was in situ monitored with reflection high energy electron diffraction (RHEED), which allows controlling the two-dimensional (2D) growth as well as the formation of QDs.

In this work, we realized samples with 1, 5, 8, 10, and 13 layers of QDs to study the impact of the number of stacks on the optical properties. The thickness of the spacer layers between the QD layers is 14 nm each. An additional uncapped top layer of QDs is realized. For this uncapped sample it is important to immediately cool down the sample after the formation of the top QDs to prevent re-evaporation of GaN. This QD top layer serves for ex situ investigations of the QD size. Measurements of uncapped as well as capped QDs are performed with atomic force microscopy (AFM) measurements.

Cross-sectional transmission electron microscopy (TEM) images are performed in a FEI Tecnai G2 F20<sup>[18]</sup> on the sample with eight layers of QDs and an additional uncapped top layer of QDs to see the correlation between the layers. The TEM lamella is prepared by splitting the sample and thinning the cross-section out by focused ion beam.<sup>[19]</sup>

Additionally, the samples are characterized optically by photoluminescence (PL) spectroscopy. The PL measurements are performed at room temperature with a Nd:YAG laser at a peak wavelength of 266 nm (energy: 4.66 eV, power: 5 mW, excitation spot diameter: 2  $\mu\text{m}$ ). A monochromator with a grating

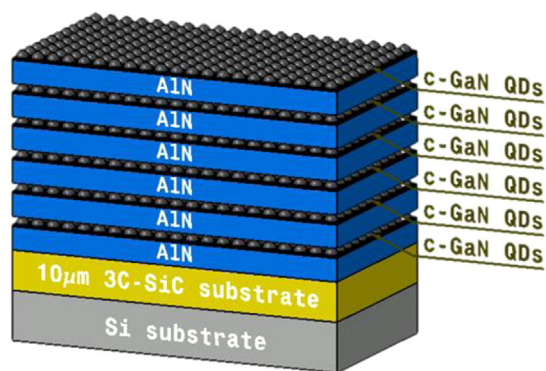


**Figure 1.** Sample structure of sample with five layers of QDs and an additional uncapped c-GaN QD layer on top. The c-AlN buffer layer and the c-AlN spacer layers have a thickness of 14 nm each.

of 300 lines per millimeter and a CCD is used to detect the PL signal.

### 3. Results and Discussion

#### 3.1. Reflection High Energy Electron Diffraction

The growth of the metastable cubic phase only occurs in a narrow parameter field, why the growth process is fully monitored with RHEED. **Figure 2(a)** shows the RHEED pattern measured at the [110] azimuth after the growth of the c-AlN buffer layer. The growth is determined by the Frank-van-der-Merwe layer-by-layer growth mode, resulting in a flat 2D surface indicated by a streaky RHEED pattern.<sup>[20]</sup> During the QD formation, the RHEED pattern (see **Figure 2(b)**) changes from a 2D streaky pattern to a three-dimensional (3D) spotty pattern (see **Figure 2(b)**). This change is due to the formation of QDs. The overgrowth of the QDs results in a rapid smoothing of the surface, after about 3 nm a streaky pattern appears again (see **Figure 2(c)**). This indicates a smooth 2D surface. The smoothing is still visible after all layers of QDs. The pattern in **Figure 2(c)** shows the c-AlN spacer layer after the fifth layer of QDs. **Figure 3** proves the consistent quality of the c-AlN spacer layers with increasing number of QD layers. Three line scans of RHEED patterns are plotted in this graph. The selected line position is marked in **Figure 2(c)** and is set in a way that the (0,1) and (0,-1) reflection can be depicted. At this position a line scan would directly show an increase of the 3D part. The sample, which is analyzed here, consists of seven layers of QDs. The constant distance of the streaky lines from the (0,-1) and the (0,1) reflections to the (0,0) reflection indicates a consistent lattice constant in each layer. The difference in intensity of the (0,1) and (0,-1) reflections is only due to our setup as well as the saturation of the main peak. The intensity of the side peaks shows a little decrease in intensity and a constant full width half

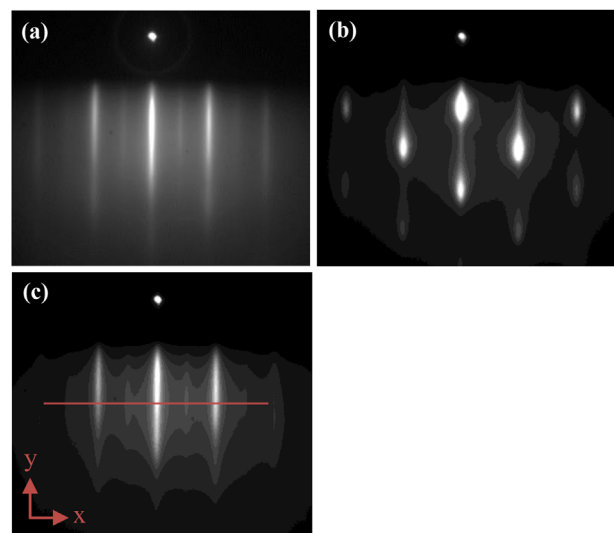


**Figure 2.** RHEED patterns measured at the [110] azimuth (a) after the growth of the c-AlN buffer layer, (b) after formation of SK QDs and (c) after the overgrowth of the fifth QD layer.

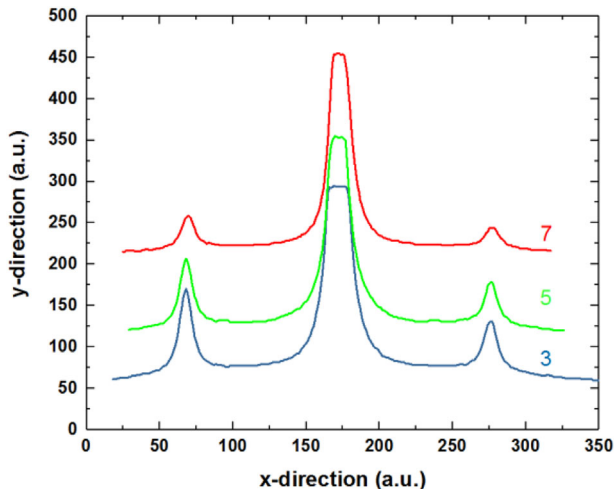


**Figure 3.** Line scans of RHEED patterns after growth of the third, fifth, and seventh spacer layer. The selected line position is shown in Figure 2(c).

maximum (FWHM). Despite the saturation of the main reflection, a decrease of intensity can be indicated, too. This overall decrease of intensity is probably due to a small increase of the roughness of the AlN layer. This must be investigated in future experiments. Nevertheless, an increase of the 3D reflections is not observable.

### 3.2. Atomic Force Microscopy Measurements

AFM measurements of both, uncapped and capped QDs are realized. The root-mean-square (RMS) surface roughness of an c-AlN covered QD sample is estimated to  $RMS = 2.1 \text{ nm}$  for a sample with five layers of QDs and a measured field of  $5 \cdot 5 \mu\text{m}^2$ . This roughness is comparable to the surface roughness of pure bulk c-AlN, which is of the same order of magnitude. This supports the observations done in the RHEED pattern, that the number of QD layers has no severe influence on the quality of the c-AlN layer.

In **Figure 4**, AFM images of the uncapped top layer of QDs are shown for the sample with 5 layers of QDs and for the sample with 13 layers of QDs. The average diameter is determined by

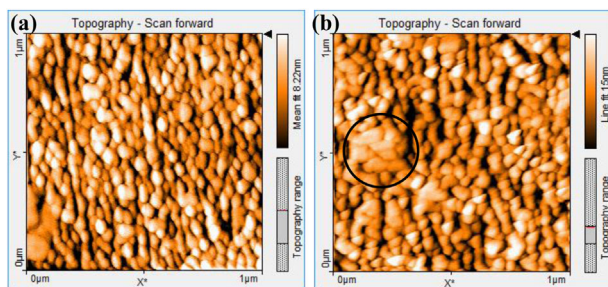


**Figure 4.**  $1 \times 1 \mu\text{m}^2$  AFM scans of the uncapped top layer of QDs of (a) a sample with five stacks of QDs and (b) a sample with 13 layers of QDs. The marked region shows agglomerated QDs.

measuring 20  $(0.5 \times 0.5) \mu\text{m}^2$  fields of each sample. Efforts are made to ensure that in the measured fields no agglomerated QDs appear like depicted in **Figure 4(b)** (black circle). Several line scans of the measured fields show an average QD diameter in all samples of  $d = 16 \text{ nm}$  ( $\pm 5 \text{ nm}$ ). The density of QDs decreases from for the sample with 5 layers of QDs to for the sample with 13 layers of QDs (see **Table 1**). In **Table 1**, the density of QDs for samples with different numbers of QD stacks are summarized.

Gogneau et al.<sup>[21]</sup> has reported a reduction of the QD density of the same order of magnitude for hexagonal self-organized GaN/AlN quantum dots. They showed a modification of shape and density up to 10 QD layers. Above the 10th period a stable configuration of the QD layers was reached. This decrease of island sizes and growth of spacing is also theoretically modeled by Tersoff et al.<sup>[22]</sup> for SiGe alloys on Si or any similar systems. If the spacing between two islands is much smaller than the spacer layer thickness, the island size and spacing becomes progressively more uniform. Islands, which are very close together, will be replaced by a single island in the subsequent QD layer. The unification of size and spacing is not visible in our samples. At this point it must be pointed out that the simulations in Ref. <sup>[22]</sup> are calculated for 2000 layers. For the case of 10 layers, the QD density is decreased, but the spacing and size is not uniform at all.

### 3.3. Transmission Electron Microscopy Measurements

In the high-angle annular dark-field (HAADF) image the QDs are clearly visible (see **Figure 5**). The QDs are vertically aligned nicely along the growth direction. The dashed line indicates the interface between the 3C-SiC substrate and the c-AlN buffer layer. The influence of the strain is visible in this TEM image. The c-AlN buffer layer with a lattice constant of  $a = 4.37 \text{ \AA}$ <sup>[23]</sup> is pseudomorphically strained on the 3C-SiC substrate with a lattice constant of  $a = 4.36 \text{ \AA}$ ,<sup>[24]</sup> because of almost the same lattice constant. Due to the lattice mismatch between c-AlN and c-GaN the c-GaN layer is compressive strained. Probably this induces a bending of the c-GaN layer. In the upper region of the image, the contrast is significantly worse. One possible reason for the low contrast is the sample preparation. As described before, the sample is cleaved to investigate the cross-sectional view of the sample. During this cleaving, the slit-plane was not exactly in growth direction. So different planes are visible in this image.

The TEM HAADF image in **Figure 6** depicts a selected region of the sample where the wetting layer is clearly visible. An additional contrast analysis of a line scan through this image from Gatan Microscopy Suite was realized as marked with the red-dashed line. For the determination of the thicknesses, half the maximum was used as transition point between AlN and

**Table 1.** QD densities for different number of stacked QD layers.

Number of layers	5	8	10	13
QD density ( $10^{10} \text{ cm}^{-2}$ )	$3.6 \pm 0.04$	$2.16 \pm 0.1$	$2 \pm 0.12$	$1.76 \pm 0.08$

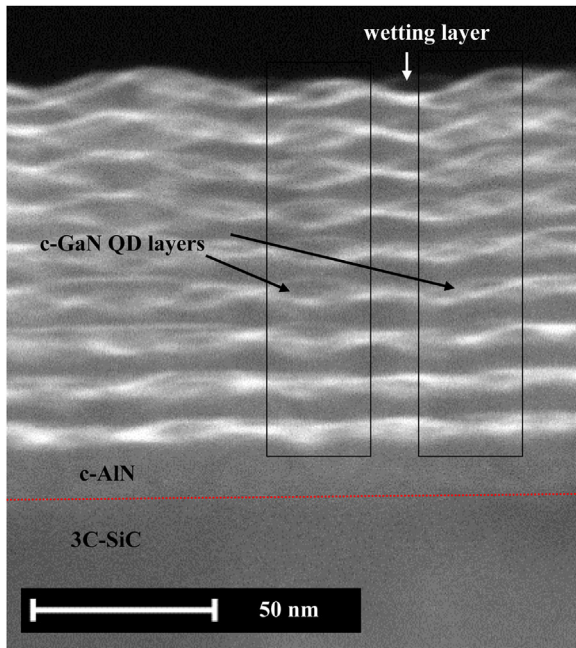


**Figure 5.** HAADF image of the sample with eight layers of QDs and an additional top layer of QDs. The red dashed line indicates the interface between 3C-SiC and c-AlN.

GaN. The results indicate that not every c-AlN layer has the desired thickness of 15 nm. The buffer layer has approximately the expected thickness of 17 nm, however, the spacer layer thicknesses are reduced to about 10 nm. The growth conditions

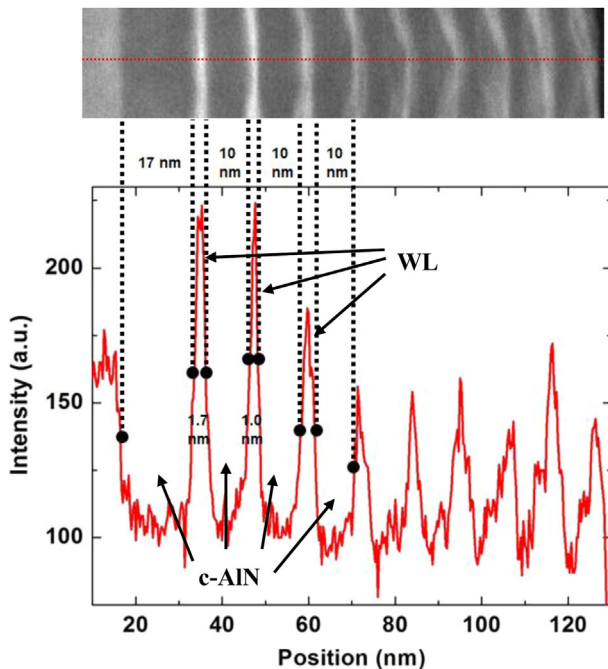


**Figure 6.** Contrast analysis of the TEM image to determine the c-AlN thickness. The upper region has been neglected, because of the low contrast ratio due to the smearing of the planes.

have not been changed, so the reason for the smaller thicknesses of the spacer layer must be related to the growth rate as already mentioned in Section 2. The upper region of the sample has been neglected, because of the low contrast. The wetting layer thickness is amounted to 1–1.7 nm (5–7 ML).

In the bright field image with atomic resolution (see **Figure 7** (a)), the wetting layer thickness is better to define due to the much higher resolution. The thickness amounts to 0.2–0.7 nm (1–3 ML). The fourth and fifth QD layers are depicted in this figure. The QD shape is like a truncated pyramid, which is already expected by Fonoberov and Balandin.<sup>[25]</sup> The truncated form is indicated with the yellow-dashed lines. The diameter of the QD is  $\approx 10$  nm and the height is 2 nm resulting in an aspect ratio of 5. In this region of the sample no stacking faults or other

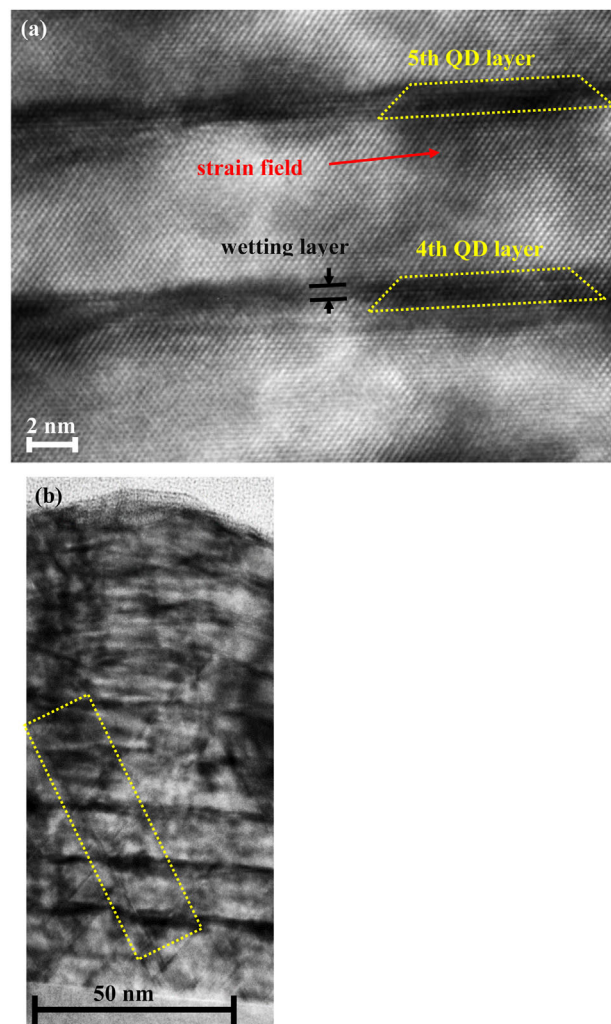


**Figure 7.** (a) Cross-sectional TEM image with atomic resolution acquired along the [110] zone axis of QD layer numbers 4 and 5. The GaN-QD and the wetting layer appear dark, the c-AlN spacer layer bright. No stacking fault is visible in this region. The yellow line indicates the truncated pyramidal shape. (b) TEM picture of a sample region with stacking faults. The area framed by dashed yellow lines shows that the vertical alignment is tilted along the [111] direction.

defects occur. The QDs are vertically aligned through the growth direction [001]. Furthermore, strain fields are observed in the surrounding of the QDs in the c-AlN layers. Due to the SK growth mode, the surrounding of the QDs is tensile strained in growth direction, whereas the QDs are compressively strained. One strain field is highlighted in Figure 7(a). Same observations were done for InAs/GaAs QDs by Heidemeyer et al.<sup>[16]</sup> Due to these strain fields the vertical alignment of the QDs occurs. It is clearly observable that the strain fields increasingly arise in the surrounding of the QDs (see dark regions highlighted in Figure 7(a)).

Usually stacking faults in the [111] planes occur in the cubic phase, which are preferential nucleation sites for QDs, because they behave like elastic potential minima on the surface. Daudin et al.<sup>[26]</sup> already showed this effect. The impact of the stacking faults is shown in Figure 7(b) at another region of the sample. Here stacking faults occur, which extend to the entire sample thickness. This causes the tilted vertical alignment of the QDs in [111] direction, along the stacking faults.

### 3.4. PL Measurements

Figure 8 shows the spectra of the PL emission of four stacked QD samples with 5, 8, 10, and 13 stacks and an additional reference sample with only one layer of QDs. It is worth noting that the excitation energy leads to direct absorption in the QDs and not in the spacer layer. Furthermore, no emission peak related to the wetting layer is observed. Dependent on the thickness of the wetting layer the transition energy for thin quantum wells is calculated to be larger than the used excitation energy of 4.66 eV and it is for that reason not visible in the PL spectra. In addition, the carriers will move to the energetically more favorable position of the QDs.

The PL emission energy of the reference sample with only one layer of QDs is 3.63 eV with a FWHM of 340 meV. This relatively wide range represents a superposition of Gaussian-shaped

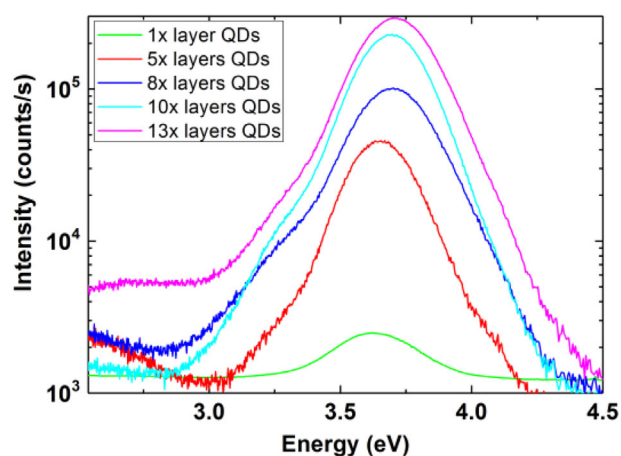


**Figure 8.** PL intensity (in logarithmic scale) versus the emission energy of the stacked QDs with 1, 5, 8, 10, and 13 layers of QDs. The measurements are done at room temperature. The emission energy and the intensity increase with increasing number of stacks.

emission bands of many individual QDs.<sup>[27]</sup> As already shown in the AFM measurements, the size of the QD varies from 11 to 21 nm. Due to the large spot size of the laser, the signal of all excited QDs results in the broad emission. The FWHM of all these samples varies slightly between 290 and 340 meV. It can be concluded that the QD distribution is comparable in all stacks. This is in contrast to observations in the hexagonal GaN QDs<sup>[20]</sup> or in other QD systems (InAs QDs) where a decrease of the FWHM with increasing number of stacked layers is found due to a homogenization of the island distribution. In our case, as homogenization of the QDs is not observed in the AFM measurements, no narrowing of the FWHM of the QW emission with increasing number of stacks is expected, which is in agreement with our PL measurements.

Figure 9 shows the dependence of the energy of the peak emission and the integral PL intensity in logarithmic scale as a function of the number of stacks. A nearly linear increase of the emission intensity with increasing number of stacks is observed. The intensity of the sample with five layers is  $\approx 40$  times as high as that of the sample with one layer of QDs. The sample with 10 layers of QDs is about 200 times as high as the sample with one stacked layer.

Stacked h-GaN QDs show a drastic increase of the PL intensity from the sample with one QD layer to the sample with three QD layers, henceforth the intensity becomes almost stable.<sup>[28]</sup> This behavior is due to the increasing uniformity of the size of the QDs with increasing layers. Up to three layers of QDs, Hoshino et al.<sup>[28]</sup> observed that the emission of large-sized QDs becomes dominant and that the formation of small QDs is drastically reduced. In our work, we presented a constant size distribution of the QDs in all samples. We conclude that this is the reason for an almost linear increase of the intensity. The presence of surface or interface properties or defects in the c-AlN has to be investigated in more detail in future. The increasing PL intensity further indicates that QDs are excited in each layer. A blueshift of the emission energy from 3.59 to 3.71 eV is determined in the PL data. In our QDs with an aspect ratio of 5 the main confining dimension is the QD height.<sup>[25]</sup> Since AFM measurements

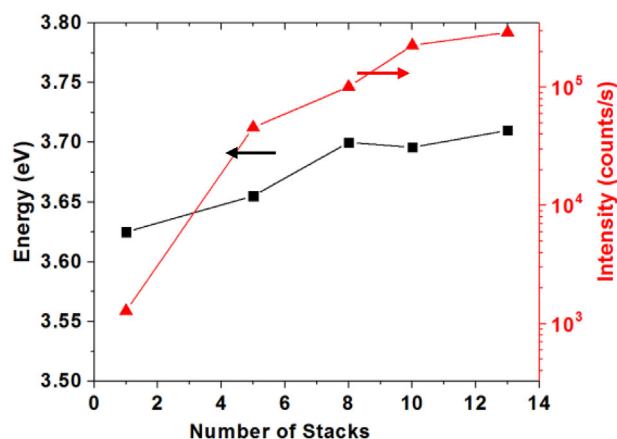


**Figure 9.** Emission energy and integrated intensity (semilogarithmic scale) as a function of the number of stacks. In both cases, an increase with increasing number of stacks is observable.

confirm that the diameter of the QDs is not modified, we assume that the blueshift of the emission energy is only due to a decrease of the QD height. Since the GaN QDs are compressively strained on the c-AlN a change of the emission energy due to strain related effects would result in a red shift of the QD emission in contradiction to our observations. Therefore, we conclude that a decrease of the QD height of one or two monolayer is responsible for the measured peak energy shift with increasing numbers of stacks.

#### 4. Conclusions

We have investigated the structural and optical properties of stacked cubic GaN QD samples. The samples are grown on 3C-SiC on top of Si (001) substrates and consist of a different number of QD layers. The self-assembled cubic GaN (c-GaN) quantum dots are grown in Stranski–Krastanov (SK) growth mode. Samples with 1, 4, 8, 10, and 13 layers of QDs embedded in cubic AlN are realized. Cross-sectional TEM measurements show that the QDs are vertically aligned along the growth direction as long as no stacking faults are nearby. In the vicinity of stacking faults the QDs are threaded along the [111] direction of the stacking faults. The QDs have the shape of a truncated pyramid with a diameter of  $\approx 10$  nm and a height of 2 nm resulting in an aspect ratio of 5. The thickness of the wetting layer is estimated to be 0.2–0.7 nm (1–3 ML).

The optical measurements show a gain of the PL intensity due to the increased number of QDs. This increase in emission intensity is almost linear and the FWHM of the PL emission is nearly independent on the number of stacks and follows no tendency. This indicates that in the cubic GaN QD case no homogenization of the QD size and shape occurs as seen in the hexagonal GaN QDs or InAs QDs. In addition, a blue-shift in emission energy with increasing number of stacked QD layers is measured. This shift is related to a decrease of the QD height (about one or two monolayers) with increasing number of stacked layers. The samples with a large number of stacked QD layers are promising candidates for applications in highly efficient UV light emitters.

#### Acknowledgments

This work was financially supported by the DFG graduate program GRK 1464 “Micro- and Nanostructures in Optoelectronics and Photonics” and the Collaborative Research Centre TRR 142 (Project A06) “Tailored nonlinear photonics: From fundamental concepts to functional structures.”

#### Conflict of Interest

The authors declare no conflict of interest.

#### Keywords

cubic crystals, GaN, molecular beam epitaxy, quantum dots

Received: October 31, 2016  
Revised: August 4, 2017  
Published online: November 30, 2017

- [1] H. Saito, K. Nishi, I. Ogura, S. Sugou, Y. Sugimoto, *Appl. Phys. Lett.* **1996**, *69*, 3140.
- [2] M. V. Maximov, Y. M. Shemyakov, A. F. Tsatsul'nikov, A. V. Lunev, A. V. Sakharov, V. M. Ustinov, A. Y. Egerov, A. E. Zhukov, A. R. Kovsh, P. S. Kop'ev, L. V. Asryan, Z. I. Alferov, N. N. Ledentsov, D. Bimberg, A. O. Kosogov, P. Werner, *J. Appl. Phys.* **1998**, *83*, 5561.
- [3] K. Hoshino, S. Kako, Y. Arakawa, *Phys. Status Solidi B* **2003**, *240*, 322.
- [4] C. Santori, S. Götzinger, Y. Yamamoto, *Appl. Phys. Lett.* **2005**, *87*, 051916.
- [5] T. Schupp, T. Meisch, B. Neuschl, M. Feneberg, K. Thonke, K. Lischka, D. J. As, *Phys. Status Solidi C* **2011**, *8*, 1495.
- [6] E. Martinez-Guerrero, C. Adelmann, F. Chabuel, J. Simon, N. T. Pelekanos, G. Mula, B. Daudin, G. Feuillet, H. Mariette, *Appl. Phys. Lett.* **2000**, *77*, 809.
- [7] M. Bürger, J. K. N. Lindner, D. Reuter, D. J. As, *Phys. Status Solidi C* **2015**, *12*, 452.
- [8] S. Kako, M. Holmes, S. Sergent, M. Bürger, D. J. As, Y. Arakawa, *Appl. Phys. Lett.* **2014**, *104*, 011101.
- [9] S. Kako, M. Miyamura, K. Tachibana, K. Hoshino, Y. Arakawa, *Appl. Phys. Lett.* **2003**, *83*, 984.
- [10] M. Bürger, M. Ruth, S. Declair, J. Förstner, C. Meier, D. J. As, *Appl. Phys. Lett.* **2013**, *102*, 081105.
- [11] S. Blumenthal, M. Bürger, A. Hildebrandt, J. Förstner, N. Weber, C. Meier, D. Reuter, D. J. As, *Phys. Status Solidi C* **2016**, *13*, 292.
- [12] S. Sergent, S. Kako, M. Bürger, S. Blumenthal, K. Tanabe, S. Iwamoto, D. J. As, Y. Arakawa, *Appl. Phys. Express* **2016**, *9*, 012002.
- [13] H. Shoji, Y. Nakata, K. Mukai, Y. Sugiyama, M. Sugawara, N. Yokoyama, H. Ishikawa, *Jpn. J. Appl. Phys.* **1996**, *35*, L903.
- [14] G. S. Solomon, J. A. Trezza, A. F. Marshall, J. S. Harris, Jr., *Phys. Rev. Lett.* **1996**, *6*, 952.
- [15] N. N. Ledentsov, V. A. Shchukin, M. Grundmann, N. Kirstaedter, J. Böhrer, O. Schmidt, D. Bimberg, V. M. Ustinov, A. Yu. Egorov, A. E. Zhukov, P. S. Kop'ev, S. V. Zaitsev, N. Yu. Gordeev, Zh. I. Alferov, A. I. Borovkov, A. O. Kosogov, S. S. Ruvimov, P. Werner, U. Gösele, J. Heydenreich, *Phys. Rev. B* **1996**, *54*, 8743.
- [16] H. Heidemeyer, S. Kiravittaya, C. Müller, N. Y. Jin-Phillipp, *Appl. Phys. Lett.* **2002**, *80*, 1544.
- [17] M. O. Lipinski, H. Schuler, O. G. Schmidt, K. Eberl, N. Y. Jin-Phillipp, *Appl. Phys. Lett.* **2000**, *77*, 1789.
- [18] M. Luysberg, M. Heggen, K. Tillmann, *J. Large-Scale Res. Facil. (JLSRF)* **2016**, *2*, 138.
- [19] M. Kruth, D. Meertens, K. Tillmann, *J. Large-Scale Res. Facil. (JLSRF)* **2016**, *2*, 105.
- [20] T. Schupp, K. Lischka, D. J. As, *J. Cryst. Growth* **2010**, *312*, 1500.
- [21] N. Gogneau, F. Fossard, E. Monroy, S. Monnoye, H. Mank, B. Daudin, *Appl. Phys. Lett.* **2004**, *84*, 4224.
- [22] J. Tersoff, C. Teichert, M. G. Lagally, *Phys. Rev. Lett.* **1996**, *76*, 1675.
- [23] T. Schupp, K. Lischka, D. J. As, *J. Cryst. Growth* **2010**, *312*, 1500.
- [24] A. Taylor, R. M. Jones, in *Silicon Carbide – A High Temperature Semiconductor* (Eds.: J. R. O'Connor, J. Smiltens), Pergamon Press, Oxford, London, New York, Paris **1960**, 147.
- [25] V. A. Fonoberov, A. A. Balandin, *J. Appl. Phys.* **2003**, *94*, 7178.
- [26] B. Daudin, G. Feuillet, H. Mariette, G. Mula, N. Pelekanos, E. Molva, J.-L. Rouvière, C. Adelmann, E. Martinez-Guerrero, J. Barjon, F. Chabuel, B. Bataillou, J. Simon, *Jpn. J. Appl. Phys.* **2001**, *40*, 1892.
- [27] S. Sergent, S. Kako, M. Bürger, D. J. As, Y. Arakawa, *Appl. Phys. Lett.* **2013**, *103*, 151109.
- [28] K. Hoshino, S. Kako, Y. Arakawa, *Appl. Phys. Lett.* **2004**, *85*, 1262.